



Asymmetrical diffusion across a porous medium-homogeneous fluid interface

J. Alvarez-Ramirez^{*}, L. Dagdug, L. Inzunza, E. Rodriguez

División de Ciencias Básicas e Ingeniería, Universidad Autónoma Metropolitana-Iztapalapa, Apartado Postal 55-534 Iztapalapa, México D.F., 09340, Mexico

HIGHLIGHTS

- Fluid–porous medium interfaces exhibit sharp geometric and diffusion transitions.
- Brownian dynamics simulations were used for studying the diffusion.
- Asymmetrical diffusion across the interface was detected.
- Asymmetries are explained by the advection-like effects at the interface.

ARTICLE INFO

Article history:

Received 30 January 2014

Received in revised form 13 March 2014

Available online 29 March 2014

Keywords:

Diffusion

Porous medium

Interface

Transport asymmetry

ABSTRACT

Interfaces formed by a homogeneous fluid and a porous media are commonly found in nature and applications. This work uses Brownian motion simulations for exploring the effects of the interface in the diffusion transport of passive particles. The results revealed that the diffusion transport is asymmetric in the sense that particles migrate faster in the porous medium-to-homogeneous fluid interface than in the opposite direction. Besides, such asymmetry is stronger as the porosity decreases. Macroscopic model using volume averaging methods showed that the asymmetrical diffusion effect is induced by sharp transitions in porosity and effective diffusivity in a vicinity of the interface.

© 2014 Elsevier B.V. All rights reserved.

1. Introduction

Many natural and practical systems with diffusive mass transport are formed by a homogeneous fluid region and an adjacent porous medium saturated by the same fluid [1]. Examples of this class of configurations are filtration processes, ground water pollution, drying processes, separation membranes, transport in biological tissues, among many others. In general, the transport properties at the fluid bulk are well understood and diverse theoretical and experimental schemes are available nowadays. On the other hand, important efforts have been devoted to the experimental [2–4] and theoretical [5–8] determination of effective diffusivities for homogeneous porous media. However, the description of the diffusion of particles around the fluid–porous medium inter-region has received less attention due to the difficulty of understanding the geometrical effects of the transition region on the effective transport parameters. In particular, sharp variations of the porous medium properties (e.g., porosity) and transport parameters (e.g., diffusivity) around the fluid–porous medium inter-region hamper the derivation of models describing the macroscopic diffusion phenomenon.

Experimental results describing the diffusion transport across fluid–porous medium interfaces are scarce. Recent experimental results have shown evidence of asymmetrical dispersive transport of conservative tracers across interfaces

^{*} Corresponding author. Tel.: +52 55 58044650; fax: +52 55 58044650.

E-mail address: jjar@xanum.uam.mx (J. Alvarez-Ramirez).

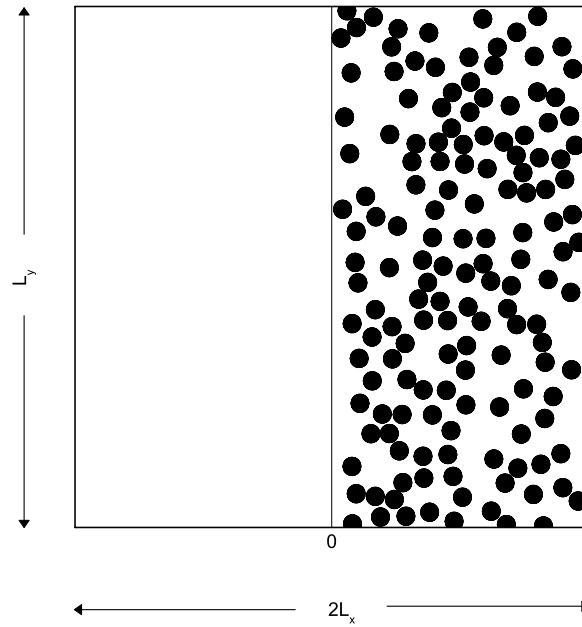


Fig. 1. Schematic diagram of the transport system. The porous medium is represented by circular obstacles with non-overlapping configuration.

between different porous materials [9,10]. Breakthrough curves showed that tracers migrating from fine medium to coarse medium arrive significantly faster than those in the opposite direction. On the other hand, some results regarding the macroscopic modeling have been reported in the recent years. The one-domain approach considers the porous medium as a continuum with effective transport coefficients, and the transition from the fluid to the porous medium is achieved through a continuous transition of properties, such as diffusivity and porosity [11]. In contrast, the two-domain approach describes the porous medium and the fluid according to the inherent properties of each region. Contrary to the one-domain approach, a model matching problem to couple the transport in both homogeneous regions needs to be addressed, resulting in the so-called jump boundary conditions [12]. These jump conditions often contain coefficients whose dependence of the local geometry of the inter-region is missing. To this end, some approximate approaches have been proposed [13]. In general, the derivation of macroscopic models for describing diffusion between a porous medium and a homogeneous fluid is made from volume averaging techniques [14], which leads to the formulation and solution of closure problems linked to effective transport parameters.

The region between a porous medium and a homogeneous fluid commonly involves sharp geometric (e.g., porosity) and transport (e.g., effective diffusivity) parameters. Despite the importance of such systems for natural and application systems, studies describing the effects of sharp transitions in the diffusion transport of passive particles are still lacking. Motivated by this, the aim of this work is two fold:

- To use Brownian random walk simulations for gaining insights in the effects of interfaces in the diffusion transport of passive particles. In analogy to recent experiments for packed columns [9], breakthrough curves show that tracers migrating from the porous medium to the homogeneous fluid arrive significantly faster than those in the opposite direction.
- To formulate a macroscopic diffusion model accounting for asymmetrical diffusion across porous medium-fluid interfaces. It is shown that asymmetrical transport can be modeled as an advection-like phenomenon induced by porosity and effective diffusivity transitions in the interface vicinity.

Overall, the results in this work indicate that transitions in the medium structure can lead to interesting transport effects that can be exploited for applications (e.g., mass transport rectification).

2. Methods

2.1. System description

The system under consideration consists of a two-dimensional saturated porous medium and a homogeneous fluid. The porous medium is composed by N_{obs} non-overlapping circular obstacles of radius R , randomly distributed in the right segment. Fig. 1 presents a schematic description of the porous medium system. Tracers are allowed to move either from the left to the right boundary or vice versa.

For a porous medium with non-overlapping circular obstacle, like that in the right-hand side in Fig. 1, the computation of porosity is an easy task. In fact, the porosity is given by

$$\varepsilon_f = \frac{L_x L_y - N_{\text{obs}} \pi R^2}{L_x L_y}. \quad (1)$$

It is noted that $N_{\text{obs}}/(L_x L_y)$ corresponds to the average number of obstacles per unit of area. In the next section, it will be required to compute the statistical variations of the porous medium porosity along the x -direction. To this end, the domain length L_x is divided into N_x vertical strips of width $\Delta x = L_x/N_x$. For each strip, the porosity should be computed and averaged over N_{conf} porous medium configurations. For porosity computation, one should consider that only sections of circular obstacles are retained within a given strip. In this way, an equation similar to Eq. (1) cannot be used. For addressing this issue, one can take advantage of the rectangular geometry of the vertical strips for estimating porosity by means of a two-dimensional, uncorrelated random sampling. This is done as follows: generate M_{ran} pairs of uniformly distributed random numbers (r_x, r_y) , with $r_x \in (x, x + \Delta x)$ and $r_y \in (0, L_y)$. The random pair (r_x, r_y) is used for sampling the strip with respect to the sections of circular obstacles retained within the strip with left and right boundaries x and $x + \Delta x$, respectively. Let $M_{\text{ran}}^{\text{obs}} < M_{\text{ran}}$ be the number of random numbers hitting the sections of the circular obstacles located within the strip considered. Then, an estimate of the porosity is given by

$$\varepsilon_f = \frac{M_{\text{ran}} - M_{\text{ran}}^{\text{obs}}}{M_{\text{ran}}}. \quad (2)$$

For a sufficiently large value of M_{ran} , the uniformly distributed pairs provides a good sampling of the obstacles contained within the strip. For obtaining a statistically significant estimate of the porosity, the estimate given by Eq. (2) is averaged over sufficiently large number, N_{conf} , of porous medium configurations. After trying some values for regular geometries (e.g., complete circles and squares), it was noted that the values $M_{\text{ran}} = 10^7$ and $N_{\text{conf}} = 10^3$ can provide accurate porosity estimates.

2.2. Simulation of Brownian tracers

The diffusion transport is simulated by overdamped Brownian particles freely moving in the fluid and being reflected by the obstacles. The overdamped dynamics of the particles is modeled by the Langevin equation

$$\frac{d\mathbf{r}}{dt} = \sqrt{2D_0} \boldsymbol{\xi}(t) \quad (3)$$

where D_0 is the bulk diffusivity, $\mathbf{r} = (x, y)$ and $\boldsymbol{\xi}(t) = (\xi_x(t), \xi_y(t))$ are zero-mean white Gaussian noises with autocorrelation functions $\langle \xi_i(t), \xi_j(t') \rangle = \delta_{ij} \delta(t - t')$ with $i, j = x, y$. The well-known Milstein algorithm was used for numerical integration of Eq. (3). Stochastic averages were obtained as ensemble averages over 10^5 trajectories. The time step was set at $\Delta t = 10^{-5}$, so that $\sqrt{2D_0 \Delta t} \ll 1$. The value $D_0 = 1$ was used for all numerical simulations. For simulating tracer particles crossing the homogeneous fluid–porous medium system, initial conditions are uniformly distributed along the entry boundary, corresponding to $x = -L_x$ (resp., $x = +L_x$) for crossing from the homogeneous fluid to the porous medium (resp., from the porous medium to the homogeneous fluid). To this end, the entry boundary are set as reflecting, while the output boundary was set as absorbing. The lower and upper boundaries located at $y = 0$ and $y = L_y$ are also considered as reflecting boundaries.

The ratio of the crossing times between the two transport directions is considered as a diffusion asymmetry; namely,

$$\alpha = \frac{\langle T_{\text{HFPM}} \rangle}{\langle T_{\text{PMHF}} \rangle} \quad (4)$$

where $\langle T_{\text{HFPM}} \rangle$ (resp., $\langle T_{\text{PMHF}} \rangle$) is the mean crossing time for transport from the homogeneous fluid to the porous medium (resp., from the porous medium to the homogeneous fluid) as computed for 10^5 tracers and averaged over 10^3 porous medium configurations with the same porosity given by Eq. (1). In this way, the value $\alpha = 1$ indicates that particles take the same average time for crossing the system in the either direction.

3. Results and discussion

In the following, for a given homogeneous fluid–porous medium configuration as described by Fig. 1, the average crossing times in the HFPM and PMHF directions will be computed by means of the procedure described previously. In principle, the obstacle radius R , and the horizontal L_x and vertical L_y lengths can affect the numerical simulation results. Since we are interested in the transport along the axial direction, it suffices fixing a sufficiently large value of L_y for reducing boundary effects. Numerical simulations for a large number of obstacle radius indicated that for $L_y \geq 5$ the estimations are hardly affected by the reflecting boundaries $y = 0$ and $y = L_y$. In this way, the length $L_y = 5$ was used for all simulations in the sequel.

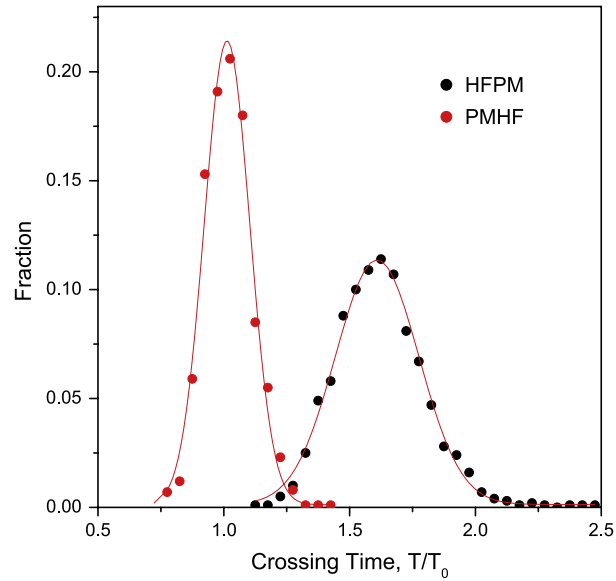


Fig. 2. Breakthrough profile for both transport directions HFPM and PMHF. The HFPM breakthrough curve has a lower peak and is broader (more disperse) than the corresponding PMHF breakthrough curve. The continuous curves are the best Gaussian fitting.

As a preliminary step, let us describe the behavior of the breakthrough curves for an illustrative example. Consider the length $L_x = 2$, the porosity $\varepsilon_f = 0.8$ and the number of obstacles $N_{\text{obs}} = 20$. The corresponding obstacle radius is $R = 0.08$. Fig. 2 presents the breakthrough profile for both transport directions HFPM and PMHF. These breakthrough curves were obtained as the distribution of the crossing times for 10^5 tracers and averaged over 10^3 random porous medium configurations. Also, the crossing times are normalized with respect to the theoretical mean crossing time for the non-porous medium, which is given by $T_0 = L_T^2/2D_0$, where $L_T = 2L_x$ is the total length to be crossed by the tracers. The breakthrough curves can be described as Gaussian distributions, which are represented by the continuous lines in Fig. 2. The HFPM breakthrough curve has a lower peak and is broader (more disperse) than the corresponding PMHF breakthrough curve. This suggests the presence of an important delay of the particles moving in the HFPM direction. In other words, tracers migrating through the homogeneous fluid segment encounter an additional resistance for crossing the interface and entering the porous medium segment. Hence, tracer accumulation at the interface causes a slow release into the porous medium segment, leading to a time delay and a more disperse breakthrough curve. The profiles of averaged tracer concentration relative to the fluid, denoted by c_f , are presented in Fig. 3. These profiles were obtained by counting the number of times the particles spend at a given horizontal position, and normalizing with respect to the number of tracers and with respect to the local porosity. The above procedure was averaged over $N_{\text{conf}} = 10^3$ porous medium configurations. It is noted that the resident concentration c_f is continuous at the interface for both directions, indicating mass conservation relative to the continuous phase (i.e., the saturating fluid) of the transport system. It should be pointed out that the average tracer concentration relative to the whole space (i.e., including obstacles), denoted by c , is commonly used for experimental measurements [10]. These average concentrations are related by $c = \varepsilon_f c_f$. Given the configuration of the transport system with sharp porosity change at the interface, it is very likely that experimental measurements of resident tracer concentration exhibit a discontinuity at sharp interfaces. However, by referring the concentration to the saturating fluid, the tracer concentration is in line with mass conservation arguments.

The effects of the radius R and the horizontal length L_x in the transport asymmetry with respect to the porous medium porosity were evaluated. For constant length $L_x = 5$ and four different values of the average number of obstacles per unit of area (i.e., $N_{\text{obs}}/(L_x L_y)$), Fig. 4(a) presents the behavior of the transport asymmetry with respect to the porosity. Recall that, for a given porosity ε_f , the relation between number of obstacles and radius is given by Eq. (1). The transport asymmetry exhibits a monotonous decreasing behavior with respect to the porosity. As more obstacles are placed within the porous medium segment, the transport asymmetry shows a slight increase for smaller porosity values. This means that tracers find increased resistance when moving in the HFPM direction than in the PMHF direction. This effect can be explained by an increase of tortuosity as an increasing number of obstacles are placed within the porous medium. As expected, in the limit as the porosity $\varepsilon_f \rightarrow 1$ (no obstacles in the right segment), the transport asymmetry vanishes (i.e., $\alpha \rightarrow 1$). For $N_{\text{obs}}/(L_x L_y) = 3$, Fig. 4(b) shows that the system length L_x has only a marginal effect in the transport asymmetry. In fact, the transport asymmetry α remains practically invariant when the axial length is increased, suggesting that the interface is the responsible of the differences of directional diffusion of tracers.

The numerical results in Fig. 4 indicate that, regardless the porous medium configuration, the transport of particles across the interface involving the homogeneous fluid and the porous medium is asymmetric. It is apparent that particles

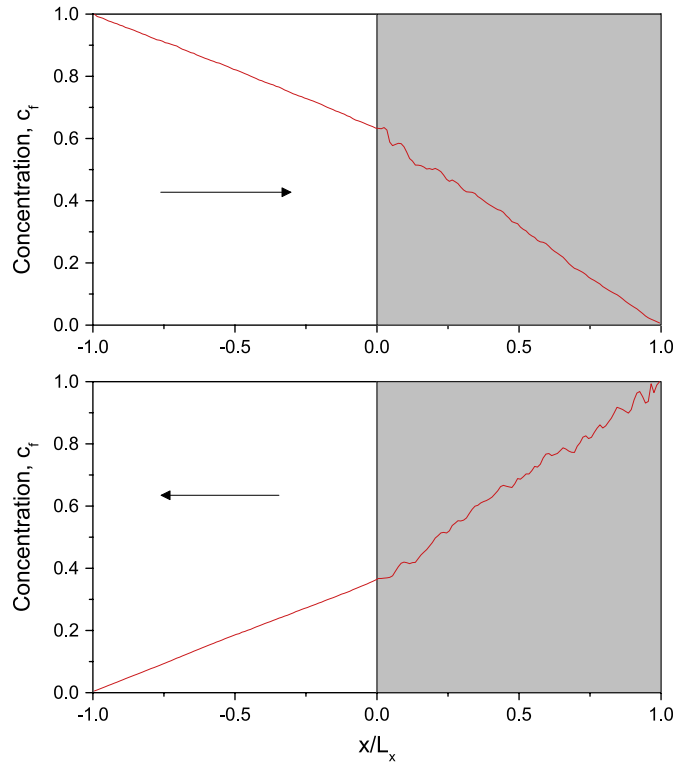


Fig. 3. Profiles of averaged tracer concentration relative to the saturating fluid, c_f .

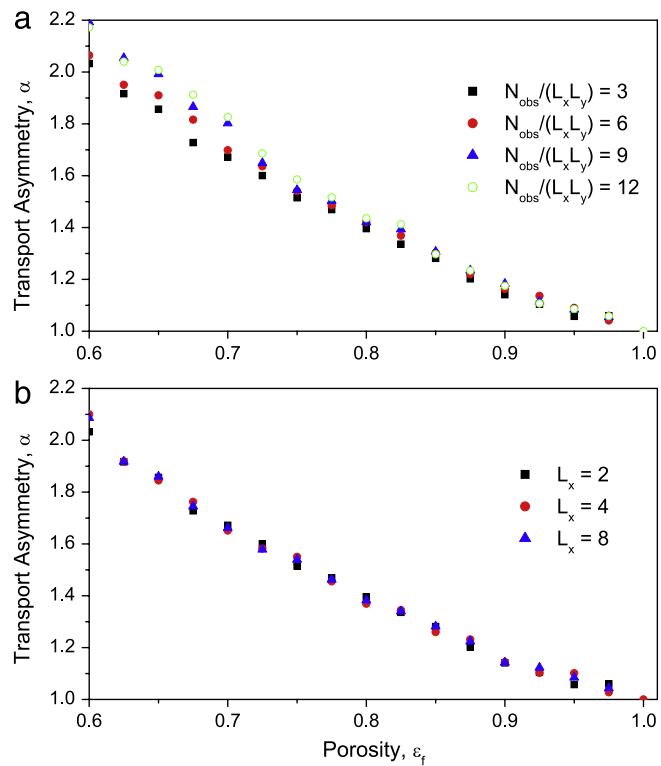


Fig. 4. Transport asymmetry with respect to the porosity as affected by (a) the number of obstacles, and (b) the axial system length. The asymmetry is higher as the porosity is decreased.

are subjected to an additional resistance when approaching the interface from the homogeneous fluid segment. The previous results have shown that heterogeneous systems with subdomains having different diffusion properties can induce asymmetries in the transport of tracers. That is, tracers move faster in some directions where trajectories find reduced resistance [15–18]. It has been shown that heterogeneous interfaces can induce an apparent drift (advection-like) effect, which can be exploited for rectification of diffusive particles [17,18].

3.1. Macroscopic modeling

Given the results described above, an interesting question is how to account for the transport asymmetry in the macroscopic modeling of the diffusion phenomenon described above. For addressing this question, the up-scaling results for diffusion in porous media described in Ref. [11] will be considered. The approach departs from considering an averaging volume, say V , for an arbitrary location of a general porous medium where diffusion transport is taking place. The use of the transport theorem [14] and the solution of a closure problem for concentration departures with respect to averaged concentrations lead to the following diffusion equation valid everywhere in the system domain:

$$\varepsilon_f(\mathbf{r}) \frac{\partial c_f}{\partial t} = \nabla \cdot (\varepsilon_f(\mathbf{r}) \mathbf{D}_{\text{eff}}(\mathbf{r}) \cdot \nabla c_f) \quad (5)$$

where \mathbf{r} is the vector of spatial coordinates within the transport system, and $\mathbf{D}_{\text{eff}}(\mathbf{r})$ is the effective diffusivity tensor, which can be obtained from the solution of a Laplace problem for some closure variables. The reader is referred to Refs. [11,14] for details of the derivation of Eq. (5). Basically, Eq. (5) describes the behavior of the averaged concentration for scales larger than the porous characteristic scale (i.e., the average porous diameter). For an isotropic homogeneous porous medium where the porosity $\varepsilon(\mathbf{r})$ is nearly constant, one has that Eq. (5) becomes a standard diffusion equation for macroscopic scales, i.e., $\frac{\partial c_f}{\partial t} = D_{\text{eff}} \nabla^2 c_f$.

In principle, one should consider the horizontal and vertical coordinates in Eq. (5) for describing the transport of tracers within the system described in Fig. 1. However, by imposing reflecting conditions at the upper and lower boundaries, it is expected that uncorrelated vertical displacements have no effects in the transport asymmetry along the axial coordinate. In this way, let us only consider the x -component of the effective diffusion tensor for obtaining the behavior of the up-scaled concentration along the axial coordinate. By doing this, one obtains the following equation constrained to the x -coordinate:

$$\varepsilon_f(x) \frac{\partial c_f}{\partial t} = \frac{\partial}{\partial x} \left(\varepsilon_f(x) D_{\text{eff}}(x) \frac{\partial c_f}{\partial x} \right). \quad (6)$$

Eq. (6) resembles the structure of the generalized Fick-Jacobs equation describing the diffusion in a symmetric channel of varying width $w(x)$. The Fick-Jacobs equation is obtained by projecting the higher-dimensional diffusion equations in one dimension measured along the centerline of the channel [19–21]. This procedure gives the following expression for the projected concentration c :

$$\frac{\partial c}{\partial t} = \frac{\partial}{\partial x} \left(w(x) D_{\text{eff}}(x) \frac{\partial}{\partial x} \left[\frac{c}{w(x)} \right] \right). \quad (7)$$

This equation shares the same structure with Eq. (6) if one uses the projected concentration relative to the saturating fluid in the channel; namely, $c_f = c/w(x)$. This leads to the following expression:

$$w(x) \frac{\partial c_f}{\partial t} = \frac{\partial}{\partial x} \left(w(x) D_{\text{eff}}(x) \frac{\partial c_f}{\partial x} \right). \quad (8)$$

In this way, the channel width $w(x)$ plays the role of the pointwise porosity $\varepsilon_f(x)$. This similarity is not surprising at all since, for a maximum channel width taken as a reference value, $w(x)/w^*$ is the pointwise fraction of the saturating fluid within the channel. The main difference between Eqs. (6) and (8) is that in the former model the pointwise effective diffusivity $D_{\text{eff}}(x)$ is estimated by solving a closure problem for a unit cell obtained from a spatial averaging problem [14], while in the latter model the effective diffusivity arises from solving the projection problem [19–21].

Estimates of spatial porosity variations can be obtained from, e.g., image processing methods. On the other hand, rather than having a direct expression for $D_{\text{eff}}(x)$, one dispose of an expression of the effective diffusivity as a function of the porous medium porosity; that is, $D_{\text{eff}}(\varepsilon_f(x))$. Fig. 5 exhibits the estimated variations of the effective diffusivity as a function of the porosity, for four different values of the average number of obstacles. Here, the porosity was controlled by increasing the radius of the obstacles. These effective diffusivity results were obtained by the standard approach of computing the slope of the mean square displacement for a given porous medium. Each estimate was obtained by averaging over the trajectories of 10^5 tracers moving in a random porous medium composed of unit cells containing N_{obs} randomly distributed circular obstacles of radius $R = \sqrt{\frac{1-\varepsilon_f}{N_{\text{obs}}\pi}}$ (see Eq. (1)). As expected, the effective diffusion is an increasing function of the system porosity. Besides, slight decrease of the effective diffusivity with the number of obstacles can be observed. This effect can be

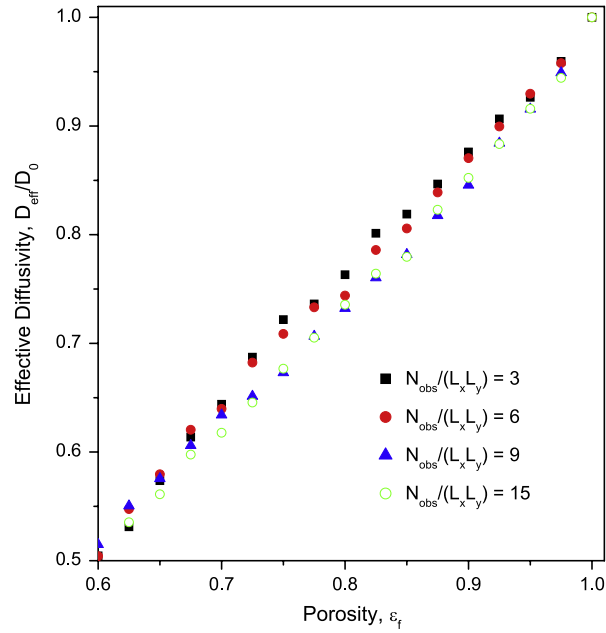


Fig. 5. Estimated variations of the effective diffusivity as function of the porosity.

attributed to an increase of the porous medium tortuosity when the number of obstacles is increased for the same porosity value. Eq. (6) can be re-written as follows:

$$\frac{\partial c_f}{\partial t} = v(x) \frac{\partial c_f}{\partial x} + D_{\text{eff}}(\varepsilon_f(x)) \frac{\partial^2 c_f}{\partial x^2} \quad (9)$$

where

$$v(x) = \frac{\left(D_{\text{eff}}(x) + \varepsilon_f(x) \frac{dD_{\text{eff}}(\varepsilon_f)}{d\varepsilon_f} \right) \left(\frac{d\varepsilon_f(x)}{dx} \right)}{\varepsilon_f(x)}. \quad (10)$$

Interestingly, Eq. (9) corresponds to an advection–dispersion model where the velocity is given by Eq. (10). One has that $\frac{dD_{\text{eff}}(\varepsilon_f)}{d\varepsilon_f} > 0$. Following the procedure described in Section 2 for porosity estimation, Fig. 6 presents an estimate of the spatial variations of the porosity at the interface vicinity for mean porosity at the porous medium bulk $\varepsilon_f \approx 0.8$. The porosity exhibits a sharp transition from $\varepsilon_f = 1.0$ in the homogeneous fluid to $\varepsilon_f \approx 0.8$ in the porous medium bulk. For the configuration described in Fig. 1, one has that $\frac{d\varepsilon_f(x)}{dx} \leq 0$. Given that $\varepsilon_f(x) > 0$ and $D_{\text{eff}}(\varepsilon_f) > 0$, one has that the velocity $v(x) \leq 0$. For the mean porosity in the porous medium bulk $\varepsilon_f \approx 0.8$, Fig. 7 illustrates the velocity field induced by porosity and effective diffusion changes in the interface vicinity. The pointwise values $D_{\text{eff}}(x)$ and $\varepsilon_f(x)$, and the corresponding derivatives $\frac{dD_{\text{eff}}(\varepsilon_f)}{d\varepsilon_f}$ and $\frac{d\varepsilon_f}{dx}$ used in Eq. (10) were computed by using cubic spline interpolation of the effective diffusivity and porosity points depicted in Figs. 6 and 7, respectively. In this way, particles migrating in the HFPD direction are subjected to a negative velocity field in the interface vicinity. In contrast, particles migrating in the HFPD direction perceive a positive velocity field, adding impulse to move faster across the interface. In turn, this velocity field leads to an asymmetry in the transport of particle across the interface.

The simple diffusion model given by Eq. (6) was numerically solved for comparing with the results obtained from Brownian tracer simulations. To this end, a normalized domain (i.e., $L_x = 1$) was considered and a central finite-difference scheme with 10^3 internal nodes was used for discretization of the spatial operator. The resulting differential equations were integrated by means of a 4/5th-order Runge–Kutta method with time step of 10^{-4} time units. No-flux (i.e., $\partial c_f / \partial x = 0$) condition was imposed at the entry boundary, and a central finite-difference was used for discretization with a ghost node. The initial condition was set as zero for all nodes, except at the entry node where a non-zero initial condition was used. In this way, similar to the Brownian dynamics simulation described in Section 2, tracers move far from the entry boundary to be detected at the opposite exit boundary. Again, cubic spline interpolation was used for estimating the pointwise values of effective diffusivity and porosity. For $\varepsilon_f = 0.8$, Fig. 8(a) presents the behavior of the breakthrough curves for the both transport directions. The vertical dotted lines depict the time location of the maximum out-through concentration. Similar to the Brownian simulation results in Fig. 2, a transport asymmetry is exhibited that reflects the faster transport in the PMHF direction than in the opposite direction. The transport asymmetry was estimated by computing the mean crossing

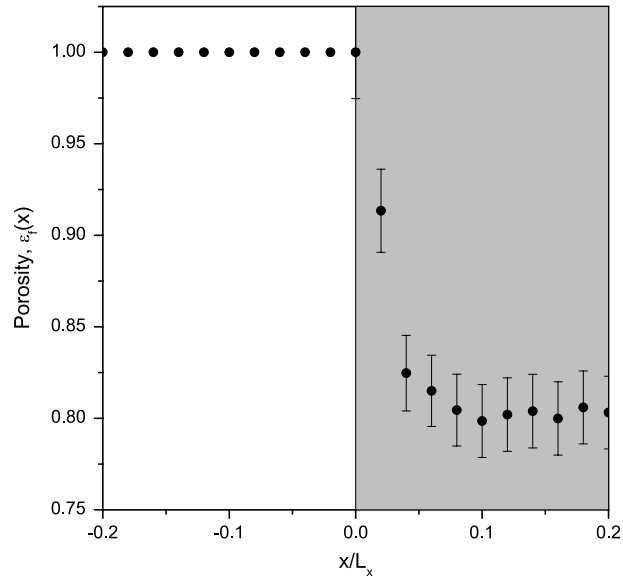


Fig. 6. Estimate of the spatial variations of the porosity at the interface vicinity, obtained by averaging over 10^3 porous configurations about $\varepsilon_f \approx 0.81$ for the porous medium bulk.

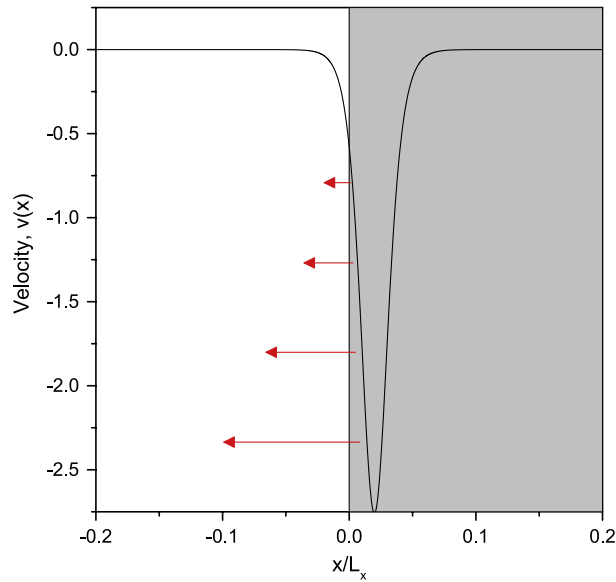


Fig. 7. Velocity field induced by the porosity and effective diffusivity transitions at the system interface. The velocity profile corresponds to the porosity variations shown in Fig. 6.

times from the breakthrough curves, and the results as function of the porosity are exhibited in Fig. 8(b). Interestingly, the estimation from the macroscopic model Eq. (6) underestimates the transport asymmetry, with maximal errors of the order of 10% for high porosity values. Overall, the previous results indicate that the transport asymmetry arises from a sort of direction-dependent resistance at the interface. In turn, the underlying physical mechanism responsible for the asymmetry of the diffusion seems very similar to the entropic bias of the fluctuations in a channel of changing section [22].

4. Conclusions

Numerical simulations of Brownian particles showed that asymmetrical transport can be induced by interfaces formed by a porous medium and a homogeneous fluid. In the vicinity of the interface, particles migrate faster in the porous medium-to-homogeneous fluid direction than in the opposite direction. Besides, the transport asymmetry is magnified as the porosity

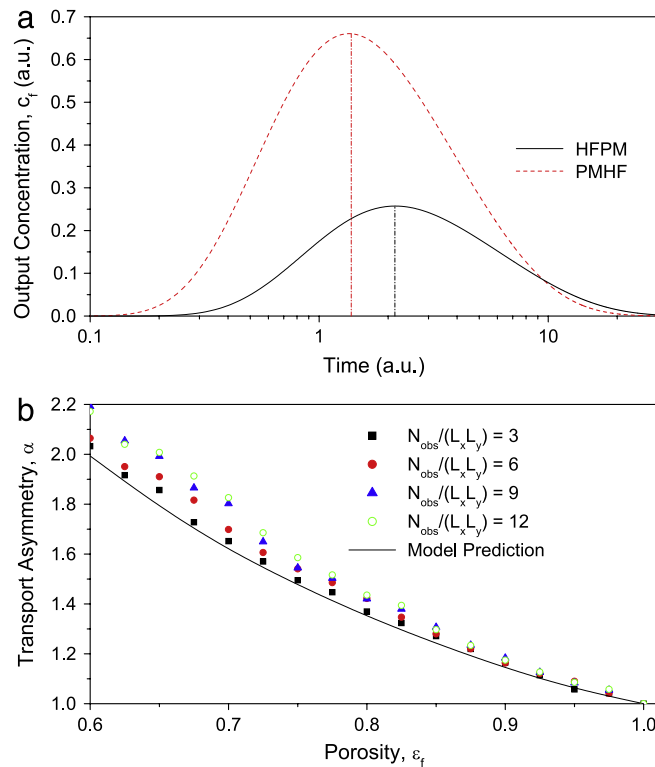


Fig. 8. (a) Breakthrough curves obtained from the numerical simulation of the macroscopic model given by Eq. (6). (b) Comparison between the predictions from Eq. (6) and the Brownian tracer simulations.

is decreased. Using macroscopic modeling from volume average up-scaling, it was shown that the transport asymmetry is induced by spatial changes in porosity, which is reflected as an advection term in the macroscopic transport equation.

References

- [1] G.S. Beavers, D.D. Joseph, Boundary conditions at a naturally permeable wall, *J. Fluid Mech.* 30 (1967) 197–207.
- [2] J. Hoogschagen, Diffusion in porous catalysts and adsorbents, *Ind. Eng. Chem.* 47 (1955) 906–912.
- [3] J.A. Currie, Gaseous diffusion in porous media: non-steady state method, *Br. J. Appl. Phys.* 11 (1960) 314–320.
- [4] J.H. Kim, J.A. Ochoa-Tapia, S. Whitaker, Diffusion in anisotropic porous media, *Transp. Porous Media* 2 (1987) 327–356.
- [5] N. Wakao, J.M. Smith, Diffusion in catalyst pellets, *Chem. Eng. Sci.* 17 (1962) 825–834.
- [6] H.L. Weissberg, Effective diffusion coefficients in porous media, *J. Appl. Phys.* 34 (1963) 2636–2639.
- [7] D. Ryan, R.G. Carbonell, S. Whitaker, A theory of diffusion and reaction in porous media, in: *A.I.Ch.E. Symposium Series No. 202*, vol. 71, 1981, pp. 46–62.
- [8] M. Quintard, Diffusion in isotropic and anisotropic porous systems: three dimensional calculations, *Transp. Porous Media* 11 (1993) 187–199.
- [9] B. Berkowitz, A. Cortis, I. Dror, H. Scher, Laboratory experiments on dispersive transport across interfaces: the role of flow direction, *Water Resour. Res.* 45 (2009) W02201.
- [10] R.C. Schwartz, K.J. McInnes, A.S.R. Juo, L.P. Wilding, D.L. Reddell, Boundary effects on solute transport in finite soil columns, *Water Resour. Res.* 35 (1999) 671–681.
- [11] F.J. Valdés-Parada, J. Alberto Ochoa-Tapia, J. Alvarez-Ramirez, Diffusive mass transport in the fluid–porous medium inter-region: closure problem solution for the one-domain approach, *Chem. Eng. Sci.* 62 (2007) 6054–6068.
- [12] J.J. Valencia-Lopez, G. Espinosa-Paredes, J.A. Ochoa-Tapia, Mass transfer jump condition at the boundary between a porous medium and a homogeneous fluid, *J. Porous Media* 6 (2003) 33–49.
- [13] M. Chandesris, D. Jamet, Boundary conditions at a planar fluid–porous interface for a Poiseuille flow, *Int. J. Heat Mass Transfer* 49 (2006) 2137–2150.
- [14] S. Whitaker, *The Method of Volume Averaging*, Kluwer Academic Publishers, Dordrecht, 1999.
- [15] P. Lancon, G. Batrouni, L. Lobry, N. Ostrowsky, Drift without flux: Brownian walker with a space-dependent diffusion coefficient, *Europhys. Lett.* 54 (2001) 28–34.
- [16] P.F. Tupper, X. Yang, A paradox of state-dependent diffusion and how to solve it, *Proc. R. Soc. A* 468 (2012) 3864–3881.
- [17] F. Marchesoni, Drift in diffusion gradients, *Materials* 6 (2013) 3598–3609.
- [18] J. Alvarez-Ramirez, L. Dagdug, M. Meraz, Asymmetric diffusion in heterogeneous media, *Physica A* 395 (2014) 193–199.
- [19] R. Zwanzig, Diffusion past an entropy barrier, *J. Phys. Chem.* 96 (10) (1992) 3926–3930.
- [20] D. Reguera, J.M. Rubi, Kinetic equations for diffusion in the presence of entropic barriers, *Phys. Rev. E* 64 (2001) 061106.
- [21] P. Kalinay, J.K. Percus, Corrections to the Fick-Jacobs equation, *Phys. Rev. E* 74 (2006) 041203.
- [22] J.M. Rubi, D. Reguera, Thermodynamics and stochastic dynamics of transport in confined media, *Chem. Phys.* 375 (2010) 518–522.